Journal of Power Sources 240 (2013) 786–795

Contents lists available at SciVerse ScienceDirect

Journal of Power Sources

journal homepage: www.elsevier.com/locate/jpowsour

Nickel nanowire network coating to alleviate interfacial polarization for Na-beta battery applications

Yingying Hu, Zhaoyin Wen*, Xiangwei Wu, Yan Lu

CAS Key Laboratory of Materials for Energy Conversion, Shanghai Institute of Ceramics, Chinese Academy of Sciences, 1295 DingXi Road, Shanghai 200050, PR China

HIGHLIGHTS

- Ni nanowire network coating on β″-alumina ceramics was designed and prepared.
- The coating greatly improves the wettability of β″-alumina by molten sodium.
- The coating alleviates the polarization at the Na/β″-alumina interface.

GRAPHICAL ABSTRACT

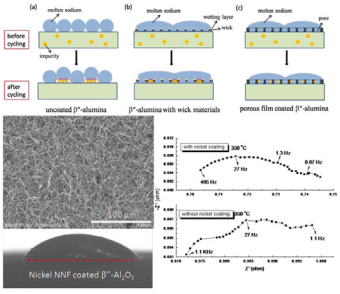

ARTICLE INFO

Article history:
Received 8 March 2013
Received in revised form
9 April 2013
Accepted 11 April 2013
Available online 21 May 2013

Keywords:
Nanowire
Network
Coating
Beta-alumina
Polarization
Sodium-beta battery

ABSTRACT

Polarization problem caused by the incomplete wetting of sodium on β″-alumina has been considered as one of the most difficult issues in Na-beta batteries. Here, nickel nanowire network coatings have been designed and fabricated directly on the β″-alumina electrolyte surface to effectively alleviate this problem. The coating consists of interconnecting nickel nanowires with diameter of about ~100 nm, forming a highly porous morphology. The structural parameters of the nickel network coatings can be tuned mainly by the amount of the poly(methyl-methacrylate) soft template in the precursors. The nickel nanowire network coatings are demonstrated to greatly improve the wettability of the β″-alumina ceramics by molten sodium. Moreover, the nickel coating displays low sheet resistance of ca. 1 Ω sq^{-1}. The results of Na/β″-alumina/Na symmetric cells at 350 °C reveal that the polarization and the interfacial resistance of the cell is alleviated intensively by the nickel coating, mainly due to the greatly improved wetting performance of the β″-alumina ceramics. This modification design and the soft-template-assisted synthetic method could be readily extended to any other substrate surfaces with arbitrary shape.

1. Introduction

As clean energy sources such as solar and wind power become more and more important, electrical energy storage systems are critical for utilization of these variable and uncontrolled energy. Recently, Na-beta batteries (NBBs) including Na–S and Na–metal halide batteries, based on a β″-alumina ceramic electrolyte that selectively allows sodium ion transport, were considered among the most promising candidates for the large capacity energy storage [1–3].

For NBBs, the molten sodium has to be maintained in contact with the full area of the β″-alumina surface, and the Na/β″-alumina interfacial polarization has to be kept to a minimum during the cell operation life. The polarization at the sodium/β″-alumina interface would be generated due to the incomplete wetting of β″-alumina by molten sodium [4,5], affecting the electrochemical performance

* Corresponding author. Tel.: +86 21 52411704; fax: +86 21 52413903.
E-mail address: zywen@mail.sic.ac.cn (Z. Wen).

0378-7753/$ – see front matter © 2013 Elsevier B.V. All rights reserved.
http://dx.doi.org/10.1016/j.jpowsour.2013.04.056

and reliability of the cell (Scheme 1). Many experimental evidences implied that one of the main reasons resulting in poor wettability was the calcium impurity in the β″-alumina ceramics, which could migrate to the sodium/β″-alumina interface during the cell cycling and might be oxidized to form a coating hampering sodium ion transport [6–8] (Scheme 2a). As demonstrated in Scheme 2b, attempts to resolve the problem have been concentrated on introducing various sodium capillary wicks and then coating the wick surfaces with high-surface-energy materials to improve the wettability of sodium on it [9–11]. In general, metals with high conductivity have higher surface energy and are more readily wetted by molten metal than other materials, considered to be one of the best choice [12,13]. As a successful example, a layer of lead significantly improved the wettability of the surface for sodium and was able to be used as a coating on the wicks [11]. Recently, thin films of Sn sputtered at the surface of β″-alumina samples under vacuum have prepared to improve the wetting of Na [14]. Our group has reported a successful method to fabricate porous carbon coatings and offered a promising solution to overcome the polarization problems of the sodium/β″-alumina interface [15]. However, the impurity migrating on the interface between the wick and the electrolyte during cycling still hinders the wetting of sodium and the sodium ion transport (Scheme 2b). Therefore, a metal network coating with thickness of micrometers prepared directly on the surface of the β″-alumina electrolyte should be a more effective route to substitute the wick materials and the corresponding wetting layer. It is proposed that the coating provided a better wetting behavior and at the same time an increased surface area to lessen the interference of impurity (Scheme 2c). However, it is a challenge to develop a low-cost simple method for the fabrication of large-scale uniform metal networks which make a close contact with the β″-alumina ceramics.

Metal nanowire networks are currently being extensively investigated and used to fabricate transparent conductive electrodes for electrode applications in devices including liquid crystal, touch panels, and solar cells [16,17]. Up to now, different methods have been applied to produce metal nanowire networks, including templateless and templating approaches [18–20]. For example, Se nanowire networks were synthesized by the vapor deposition of selenium and subsequent crystallization [18]. Metal nanowire thin coatings with hierarchical pore structure were electrodeposited by Wang et al. using mesoporous silica containing colloidal silica particles as templates [19]. Recently, scalable Ag nanowire coating on plastic substrate was fabricated through a Meyer rod coating technique [17]. However, these methods suffer from the difficulties of mass production, demanding conductive substrates or high cost, especially for the fabrication of large-scale metal network coatings on a nonconductive substrate.

Here we report a new soft-template method to produce large-area metallic nickel nanowire network coatings (NNCs) on β″-alumina ceramic substrates to improve the wettability of the β″-alumina for sodium, making it possible that the entire surface of the β″-alumina electrolyte is active. The interfacial resistance between sodium and the electrolyte obviously decreases due to the enhanced wetting, and hence the polarization behavior of the Na/β″-alumina/Na cells is greatly alleviated.

2. Experimental

2.1. Materials

Nickel oxalate dihydrate, ammonium hydroxide solution (25% as ammonia) and *N*,*N*-dimethylformamide (DMF) were purchased by Sinopharm Chemical Reagent Co. Ltd (China), while poly(methylmethacrylate) (PMMA) (average particle size: 59.7 μm) was from Aladdin Reagent Co. Ltd (China). β″-alumina ceramic (Φ16.4 mm × 1.5 mm), from Shanghai Institute of Ceramics, Chinese Academy of Sciences [21], had a chemical composition of 9.0 wt% Na_2O + 0.72 wt% Li_2O, with the balance being alumina and a β″ content of >99%; the relative density was >99%. The β″-alumina ceramics were pretreated by sonication in anhydrous ethanol successively and dried in air at 100 °C for 5 h, then stored in a drying cupboard for later use.

2.2. Nickel nanowire network coating preparation

A controlled amount of PMMA and 0.005 mol nickel oxalate dihydrate were completely dissolved in 15 mL DMF and 6 M ammonium hydroxide aqueous solution to form a homogeneous solution, respectively. Then the PMMA DMF solution was added into the nickel salt solution slowly under stirring. The mixture was kept at room temperature for 24 h with constant stirring to obtain the precursor slurry. The slurry was then cast onto the β″-alumina ceramic discs, followed by drying to obtain the precursor layer. For the tubes, we used a dip-coating process. Finally, the cast ceramics were calcined at 550 °C under N_2 atmosphere for 2 h. In order to optimize the structure of the network coatings, samples were

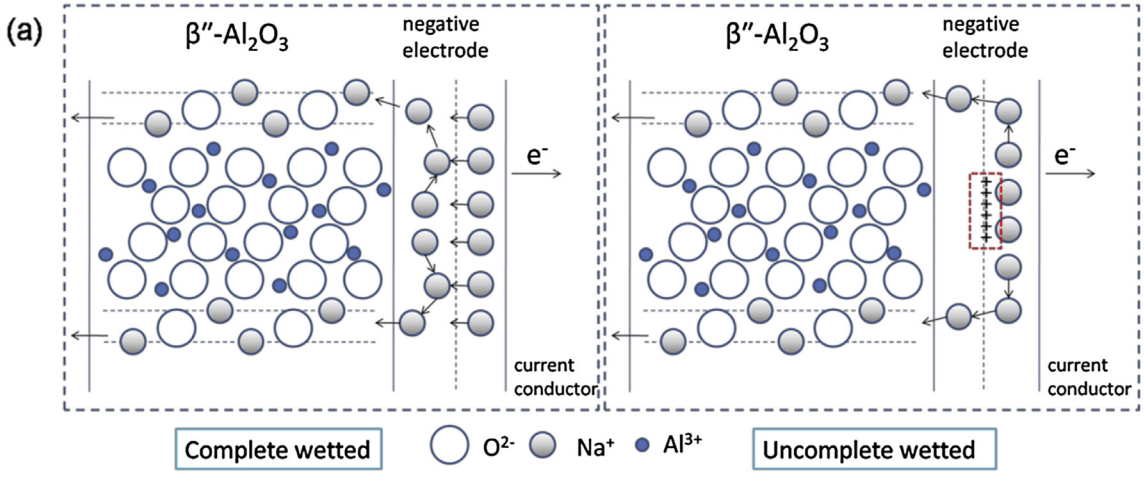

Scheme 1. Schematic representation of the interfacial polarization between sodium electrode and the β″-Al_2O_3 electrolytes.

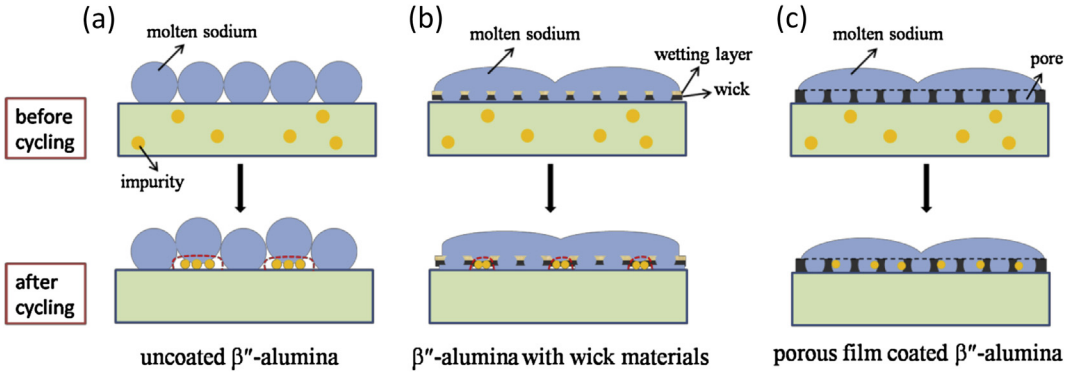

Scheme 2. Schematic representation of the wetting behavior between sodium electrode and the β″-Al_2O_3 electrolytes with and without modification by wick materials or porous metal coatings.

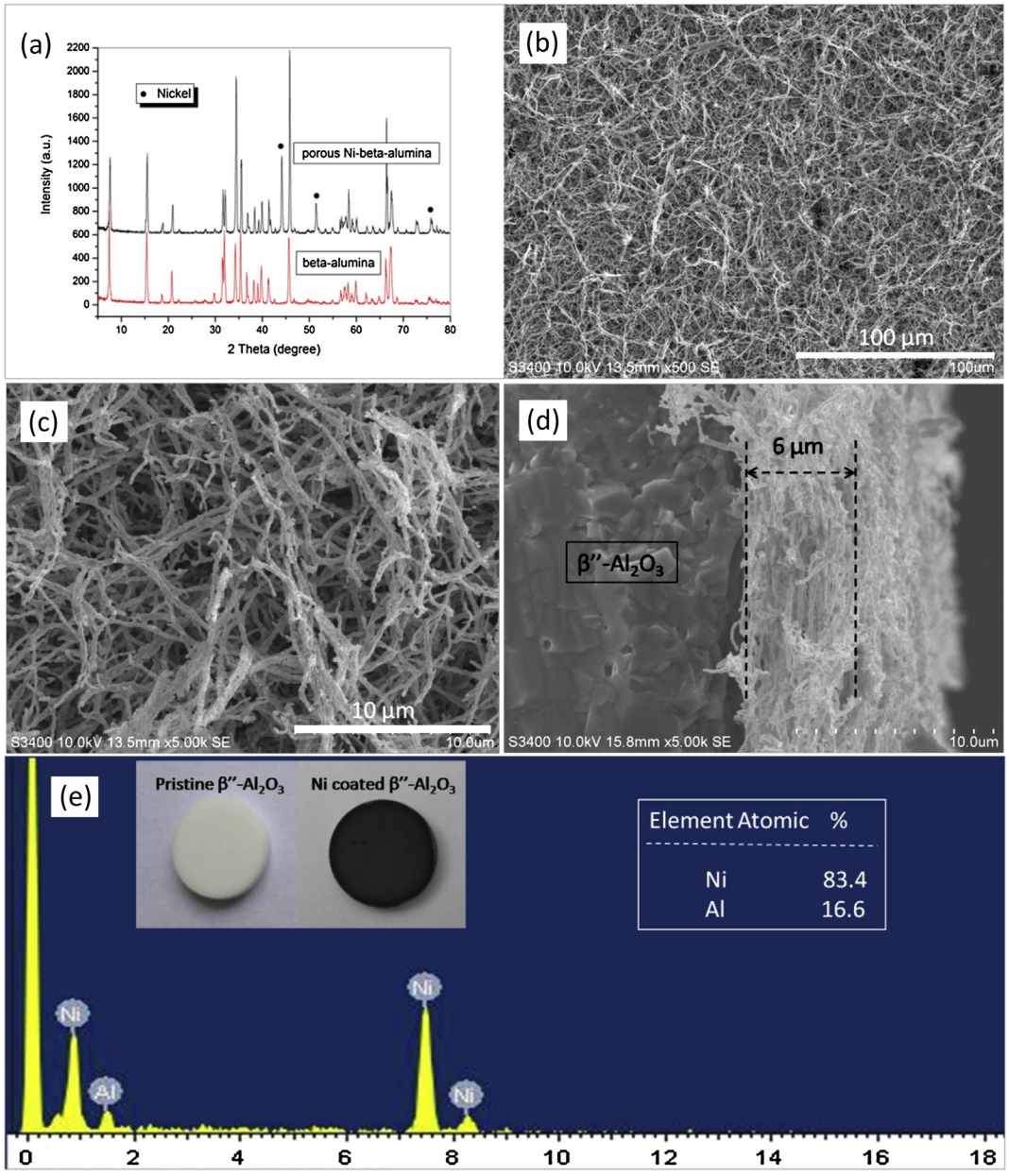

Fig. 1. (a) XRD patterns of β″-alumina ceramics with and without nickel coating. (b, c) Low- and high-magnification SEM image of nickel nanowire network coating coated β″-alumina ceramics. (d) A typical cross-sectional image of the coating. (e) the EDS pattern of the coated β″-alumina. Inset is the photographs of a β″-alumina substrate (Φ16 mm) before and after coating nickel NNC.

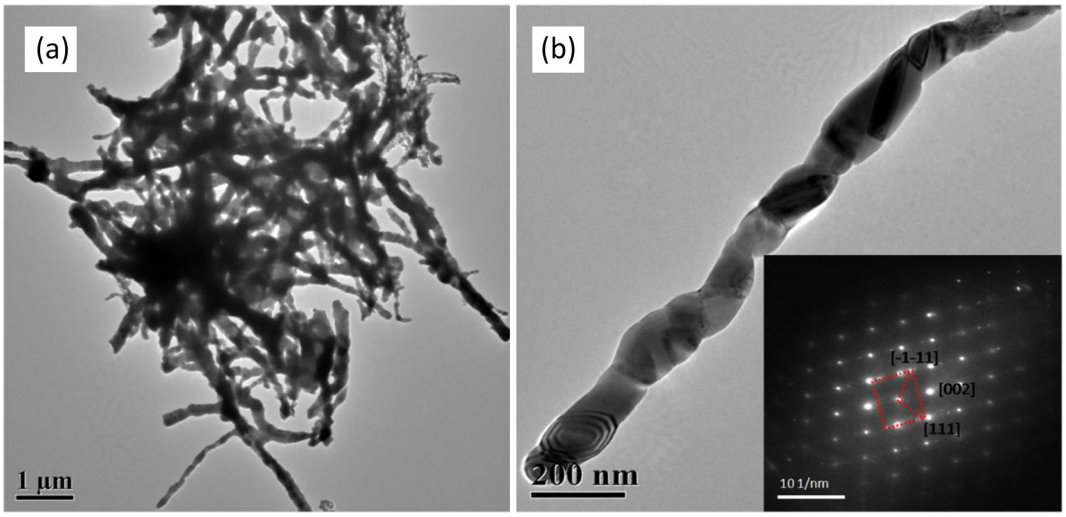

Fig. 2. TEM images of the nickel nanowires scratched from the coated β″-alumina. Insert in part b is the SAED pattern.

prepared with different PMMA amounts: 0.1 g, 0.2 g, 0.3 g, and 0.4 g.

2.3. Characterization

The nickel NNCs on the β″-alumina substrate were directly characterized by X-ray diffraction (XRD) (Rigaku Ultima IV, Cu Kα radiation, $\lambda = 1.5418$ Å), scanning electron microscopy (SEM) (Hitachi S-3400N, 15.0 kV), and transmission electron microscope (TEM and HRTEM) (JEOL-JEM 2010 type, 100 kV). Fourier transform infrared (FTIR) spectra were recorded on a Bruker Tensor 27 operating in transmittance mode at normal incidence, using a spectral resolution of 4 cm^{-1}. Thermogravimetry-differential scanning calorimetry (TG-DSC, NETZSCH 409 PC) was carried out on well ground coatings in flowing nitrogen atmosphere with a heating rate of 5 °C min^{-1}. The sheet resistances were measured in an Accent HL5500 Hall System at room temperature.

2.4. Wettability test and electrochemical measurements

The wettability examination was carried by Krüss EasyDrop at 300 °C in an argon-filled glove box for 10 min (Mikrouna Universal (2440/1000)) with oxygen and water contents lower than 1 ppm. All the samples were photographed and the contact angle was determined by a computer-supported tester. Electrochemical measurements were carried out using symmetry-electrode cells with sodium metal as the electrodes and β″-alumina ceramics with and without modifying the nickel NNCs as the electrolytes. The cell assembly was performed in vacuum environment. The cyclic

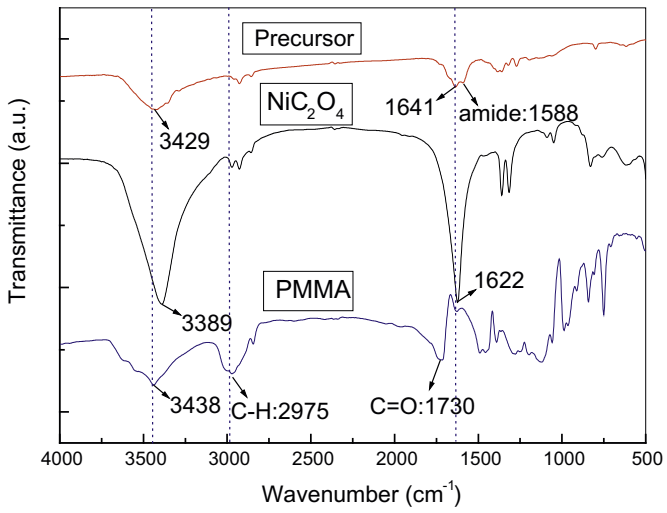

Fig. 3. FTIR spectra of the (a) PMMA, (b) NiC_2O_4 and (c) the nickel salt/PMMA composite precursor.

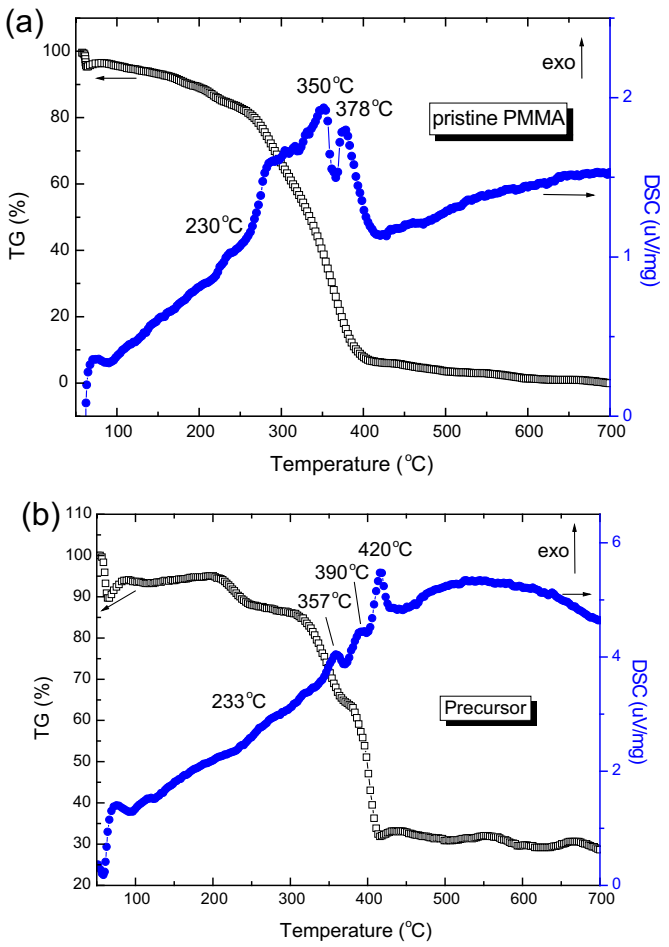

Fig. 4. TG-DSC analysis of the (a) PMMA and (b) the nickel salt/PMMA composite precursor.

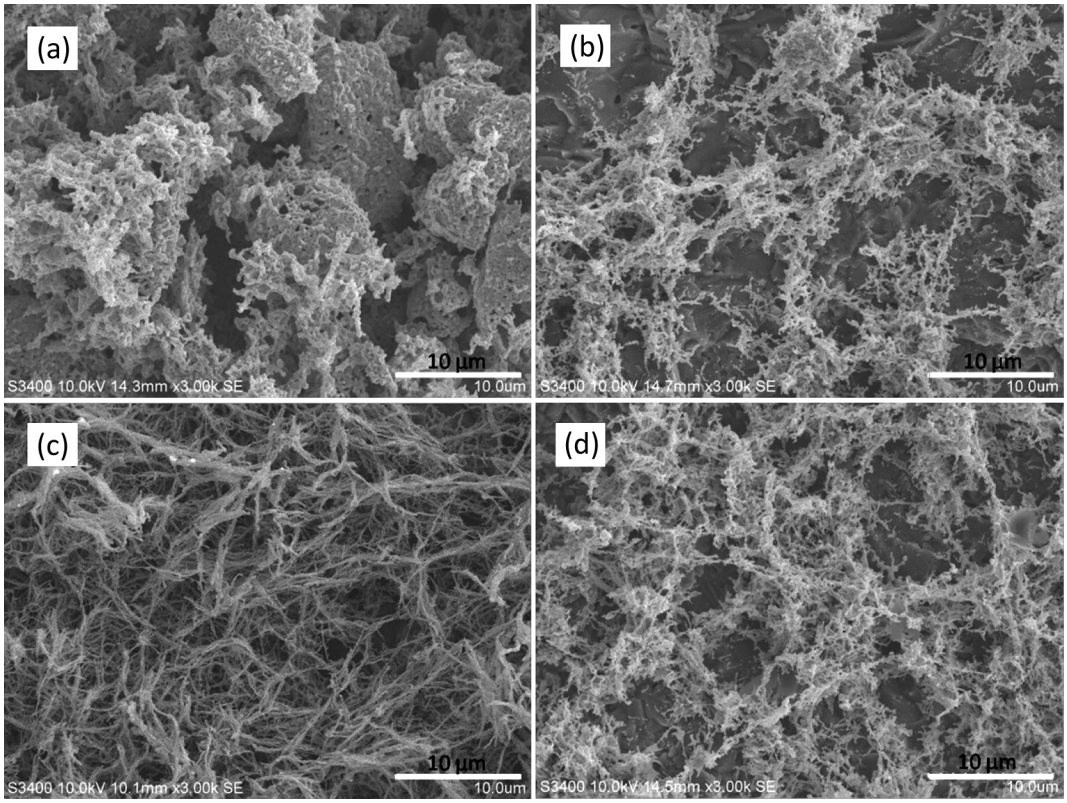

Fig. 5. SEM images of various nickel NNC coated β″-alumina ceramics obtained with (a) 0.1 g, (b) 0.2 g, (c) 0.3 g, and (d) 0.4 g PMMA.

voltammograms (CVs) were measured at the scan rate of 50 mV s^{-1} at a temperature of 350 °C. Electrochemical impedance spectroscopy (EIS) measurements were conducted using a frequency response analyzer (Autolab PGSTAT302N) with an electrochemical interface (Autolab 4.9) in the frequency range from 1 MHz to 0.01 Hz, and the fitting was performed with Nova 1.8 software. The Q value in the equivalent electrical circuit used to describe an imperfect behavior of a reactance is a constant-phase element, and the corresponding impedance could be equivalently written as

$$Z_Q = 1/[Y_o(jw)^n]$$

where j is the square root of -1, w is frequency, and Y_o and n are fitting parameters.

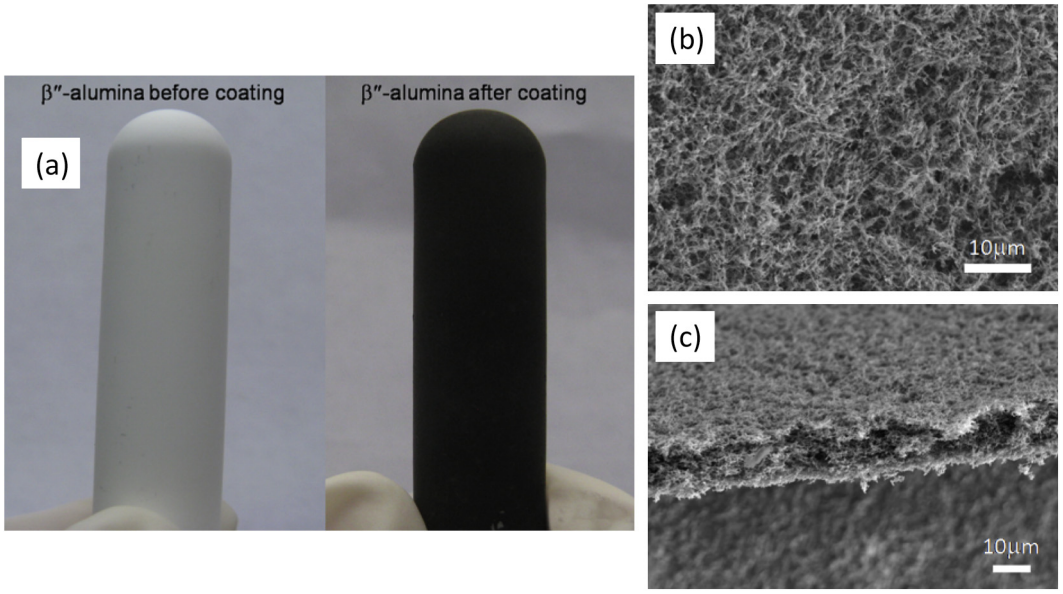

Fig. 6. (a) The photographs of a β″-alumina tube (Φ12 mm × 40 mm) after and before nickel nanowire network coating. (b,c) Top-view and cross-sectional SEM images of the film on the tube.

3. Results and discussion

Typical XRD patterns of the nickel coating coated β″-alumina and the pristine one are shown in Fig. 1a. Clearly, all the peaks of the coated sample can be indexed to cubic nickel (JCPDS Card No. 04-0850) except for those arising from the β″-alumina substrate. Fig. 1b illustrates the low-magnification SEM image of the nickel coating. The image reveals that the product exhibits large-area network structures with uniform growth density. The enlarged image in Fig. 1c demonstrates that the nickel nanowires with diameter of about ~100 nm are interconnected with each other, forming a highly porous morphology. The cross-sectional image of the network coating is shown in Fig. 1d, which shows that the average length of the uniform nickel NNC is ~6 μm. Moreover, the nickel NNC on the β″-alumina surface exhibits a noninvasive modification. The EDS result (Fig. 1e) confirms the formation of metallic nickel. The optical image of the nickel NNC is illustrated in the up-left insert of Fig. 1e (left: pristine β″-alumina; right: β″-alumina after coating nickel NNC). It shows that the as-obtained nickel NNC on a circular β″-alumina ceramic is macroscopically uniform. Further structural characterization of the nickel network was performed by TEM. Fig. 2a shows a TEM image of several individual nickel nanowires. The dimensions of the nanowires under TEM observation are in good agreement with the SEM results. From the TEM and SAED image of an individual nanowire in Fig. 2b, it confirms that nickel with single-crystal nature is the fundamental unit of the nanowire.

For the growth of the nickel NNC, a molecular-level connection between the main source and pore-forming agent was reported to be determinative [12,22]. FTIR spectra of the poly(methylmethacrylate) (PMMA), NiC_2O_4, and precursor were taken to prove the effective connection in our work (Fig. 3). Three distinct peaks appear at 3438, 2975, and 1730 cm^{-1} for pure PMMA, corresponding to the O—H stretching vibrations, the C—H asymmetrical stretching mode, C═O asymmetric stretching of the carbonyl group, respectively [23–25]. With the addition of nickel salt to

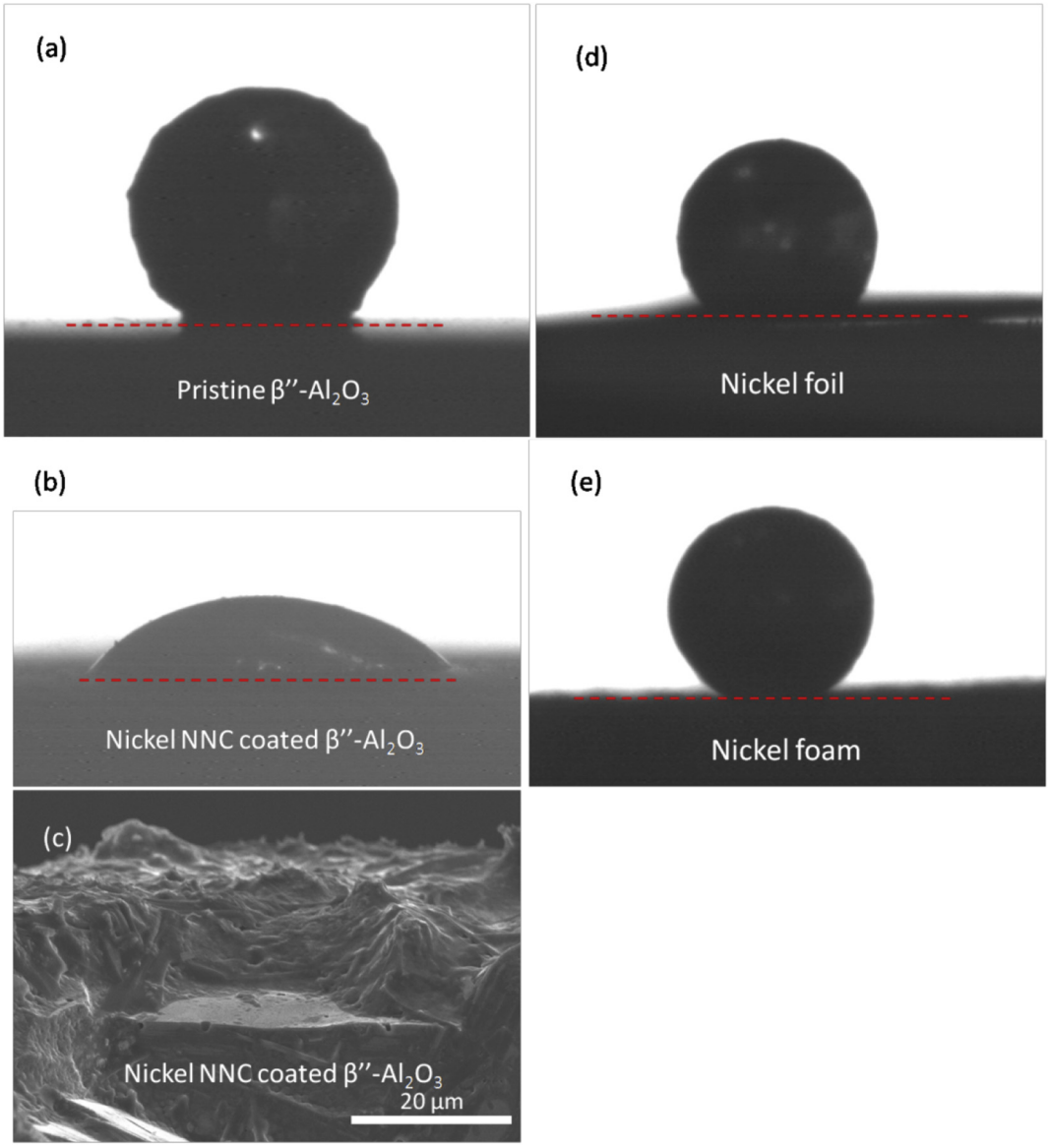

Fig. 7. Optical micrographs of the static sodium drop on (a) pristine β″-alumina, (b) nickel NNC coated β″-alumina, (d) nickel foil, and (e) nickel foam at 300 °C. (c) The cross-sectional image of the nickel NNC after the wettability test.

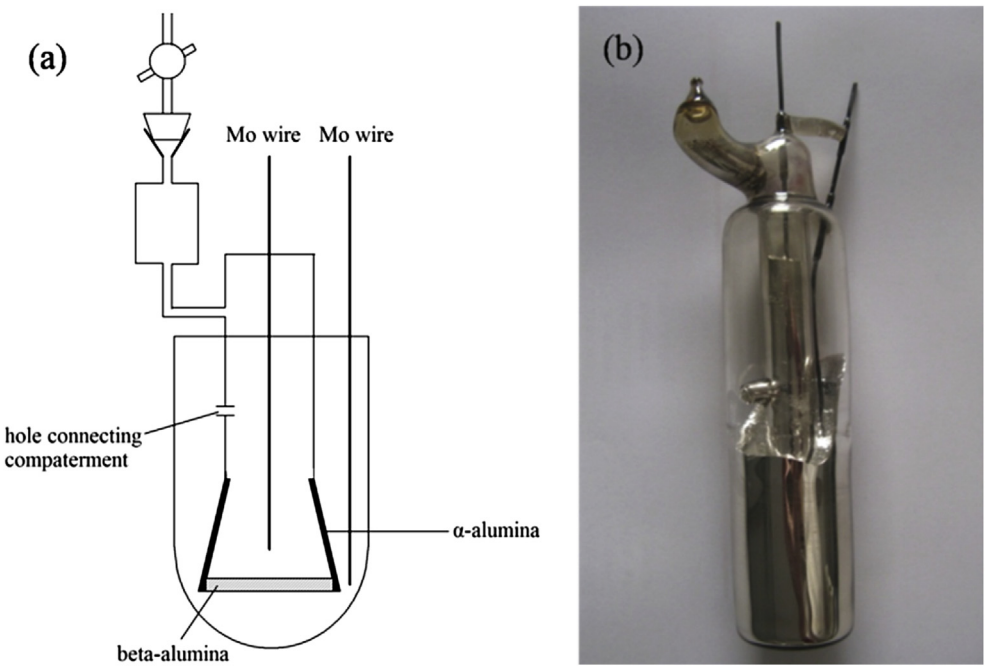

Fig. 8. (a) Schematic diagram of the Na/β″-alumina/Na cell assembly. (b) The photograph of the assembled Na/β″-alumina/Na cell.

PMMA, the peak for the O–H stretching broadens and shifts to lower wave numbers, at the same time, the C–H and C=O stretching bands disappear, indicating that there is an interaction between the PMMA and nickel salts via a coordinate bond [23]. Besides, the FTIR spectrum of pure nickel oxalate dihydrate was observed. The peak at 1622 cm^{-1} corresponding to the conjugated C=O stretching band seems to shift to 1641 cm^{-1} in the complexes, which can be ascribed to the change of the environment of oxalate

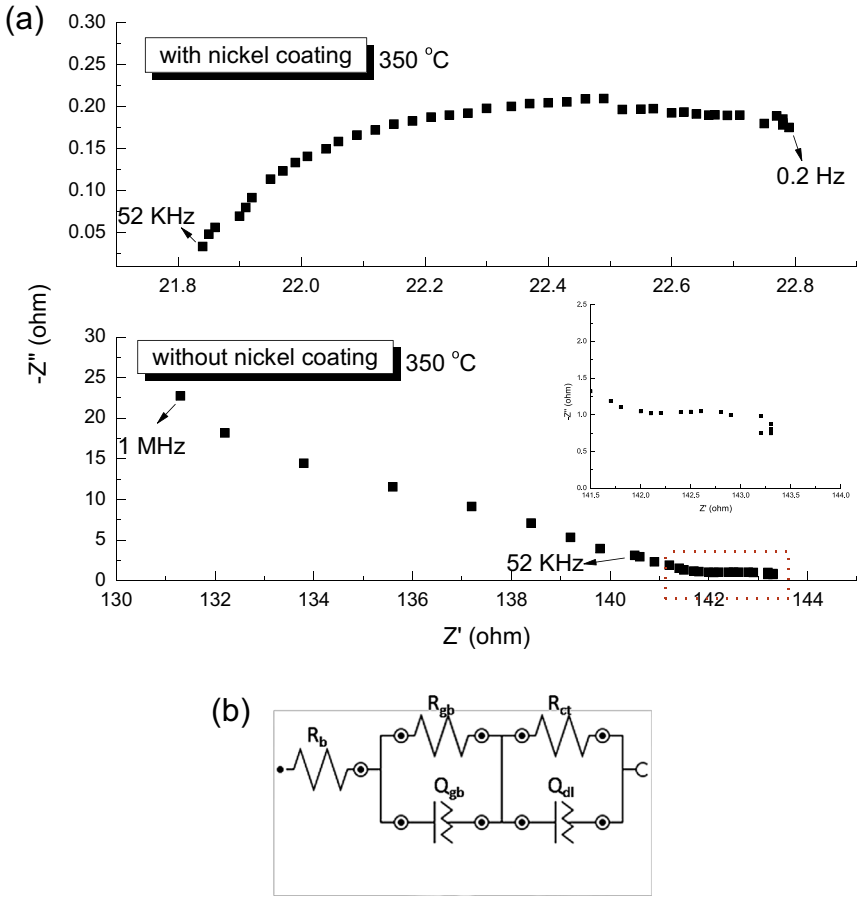

Fig. 9. Impedance spectra of Na/β″-alumina/Na with and without the nickel coating at 350 °C during the heating process. (b) Corresponding fitted equivalent electrical circuit.

ions in the complex. These results confirm good dispersion of PMMA, which finally causes the formation of the uniform nickel NNC. The thermal treatment processes of the PMMA and synthesized precursors were also studied with TG-DSC (Fig. 4). As seen, the onset temperature at about 5% weight loss is similar (70 °C for PMMA, and 65 °C for precursors), which is attributed to the evaporation of adsorptive water. The mid-point temperature of the precursor (233 °C) is increased a bit compared to pristine PMMA (230 °C). There is a sharp weight loss of 79% between 275 and 430 °C with two endothermic peaks at 350 and 378 °C, corresponding to the decomposition of PMMA. For the precursor, the two endothermic peaks shift to 357 and 390 °C, which suggests the formation of an effective connection between PMMA and nickel salt, in agreement with the FTIR results and previous observations on PMMA composites [26]. The characteristic temperature (420 °C) in the DSC curve of the precursor may be ascribed to the decomposition of the nickel salt. The weight loss between 430 and 700 °C is very little, which shows that the PMMA and precursors could decompose completely after sintering at 430 °C. Based on the above results, it is proposed that the formation of the uniform nickel NNC is mainly attributed to the connection between the pore-forming agent PMMA and nickel salt.

The concentration of PMMA in the precursors should be a key factor for controlling the generation of the nickel NNC. The SEM images in Fig. 5 illustrate the morphology of the products obtained with 0.1 g, 0.2 g, 0.3 g, and 0.4 g PMMA, respectively. As shown in Fig. 5a, the sample prepared with 0.1 g PMMA consists of only aggregated small particles. An increase of the PMMA concentration leads to the formation of the nanowires. When 0.2 g PMMA is used, particles and nanowires can be observed simultaneously (Fig. 5b). As PMMA is increased to 0.3 g, the uniform nanowire network is formed on the surface of the substrate, as illustrated in Fig. 5c. With a further increase in the PMMA concentration, the sample maintains the wire shape, but tends to form loose, porous clusters (Fig. 5d).

Besides the β″-alumina discs, since the method has no special requirements for the substrate, it seems that this process can be applied to any compact substrate with arbitrary shape that is stable under medium temperature. As an example, nickel NNC has been successfully prepared on the surface of a β″-alumina tube which is more practical in the Na-beta batteries (Fig. 6). The figure shows that the as-obtained nickel NNC on the β″-alumina tube is macroscopically uniform and mechanically robust.

The equilibrium contact angles of molten sodium on the pristine β″-alumina and nickel NNC coated β″-alumina were evaluated in an argon-filled glove box at 300 °C. As shown in Fig. 7a and b, the pristine β″-alumina represents almost non-wetting condition for sodium, in accordance with the previous reports [27], whereas the sodium droplet on the modified β″-alumina became flat with a contact angle of ~40°. Therefore, the noninvasive modification of the β″-alumina surface by nickel NNC coating remarkably improves its wettability by molten sodium. Fig. 7c shows the cross-section image of the coating after the wettability test. It can be seen that sodium can penetrate evenly into the nickel networks and make contact with the β″-alumina surface directly, which is important for

Table 1
Optimized resistances in the equivalent circuit of the Na/β″-alumina/Na cells with and without the nickel coating before and after polarization.

Na/β″-alumina/Na cell	Temperature (°C)	R_b (Ω)	R_{gb} (Ω)	R_{ct} (Ω)
Before polarization				
Without the nickel coating	350	120.5	20.5	2.8
With the nickel coating	350	21.8	0.23	0.89
After polarization				
Without the nickel coating	350	0.97	0.01	0.02
	200	2.87	0.048	0.095
With the nickel coating	350	0.696	0.043	0.007
	200	0.881	0.055	0.01

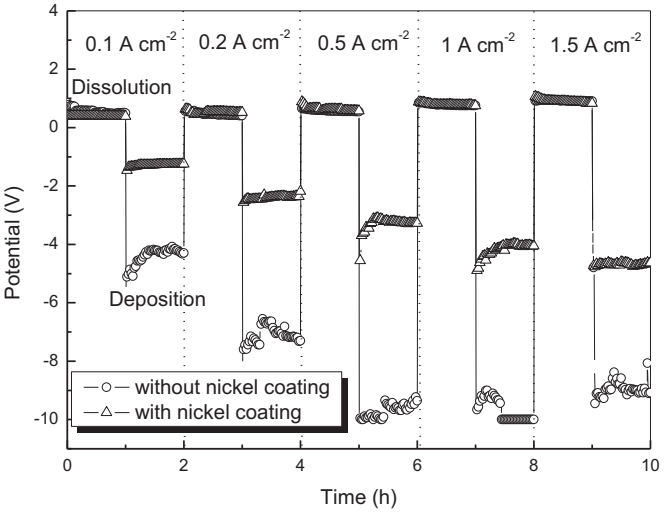

Fig. 10. Constant current polarization curves of Na/β″-alumina/Na cell with and without the nickel coating at 350 °C.

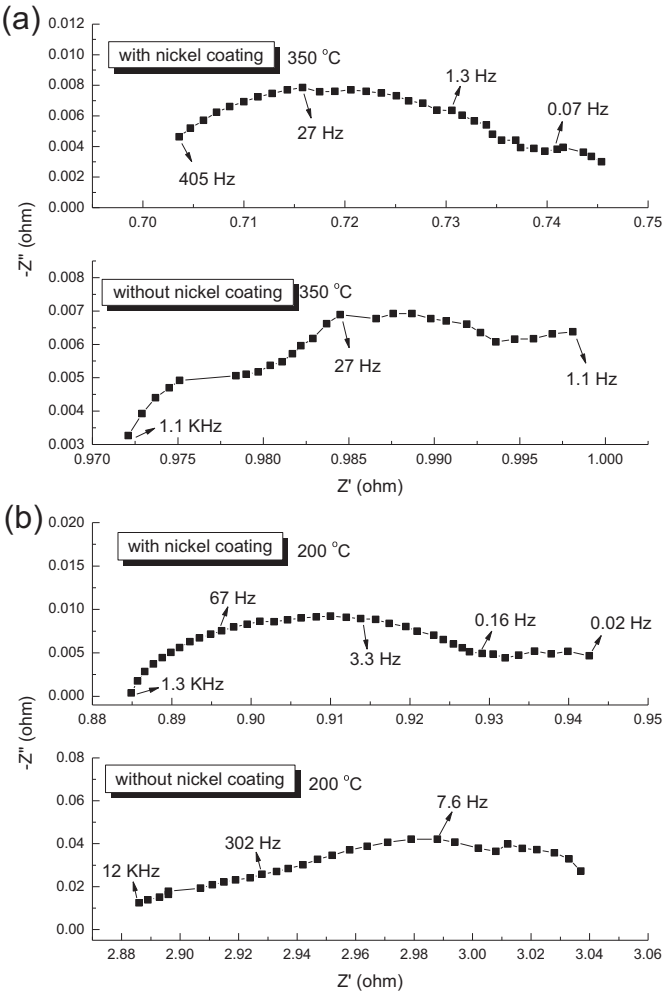

Fig. 11. Impedance spectra of Na/β″-alumina/Na with and without the nickel coating (a) at 350 °C and (b) 200 °C during the cooling process.

the electron and sodium ion transport. In addition, the wettability of sodium on nickel foil and foam are displayed in Fig. 7d and e. Both nickel foil and foam show poor wettability for sodium, illustrating that the enhanced wetting behavior partly depends on the nanoscale morphology of the coating. Furthermore, the sheet resistance of the network coating we measured is as low as ca. 1 Ω sq^{-1}.

Na/β″-alumina/Na symmetric cells with and without the nickel NNC obtained with 0.3 g PMMA were assembled to identify the effect of the nickel coating on the interfacial and polarization properties of the sodium/β″-alumina system (Fig. 8). The cells are heated to 350 °C at a rate of 1 °C min^{-1} and kept at 350 °C for 1 h, then prepared to be tested. Impedance spectra of the cells with and without the nickel NNC at 350 °C are shown in Fig. 9a. The optimized resistances in the equivalent circuit in Fig. 9b to which the impedance spectra were fitted are listed in Table 1. These impedance spectra show an intercept R_b on the real axis, corresponding to the bulk resistance of the β″-alumina, a semi-circle in the high frequency range derived from the grain boundary resistance (R_{gb}) of the β″-alumina electrolyte and a semi-circle at lower frequencies generated by the interfacial resistance (R_{ct}). The interfacial resistance of the cell without coating, when the temperature rises to 350 °C, is found to be much higher than that of the cell with coating, which can be explained by the nickel coated β″-alumina already wetted by molten sodium instead of the uncoated one. The polarization potentials of the Na/β″-alumina/Na cells with and without the nickel coating were measured at 350 °C as a function of the current density in Fig. 10. The cell without coating shows obvious polarization at a low current density (0.1 A cm^{-2}). At higher current densities (>0.2 A cm^{-2}), the potential of the cell without coating becomes unstable with time, showing an enhanced polarization. However, the cell with coating shows stable potential value

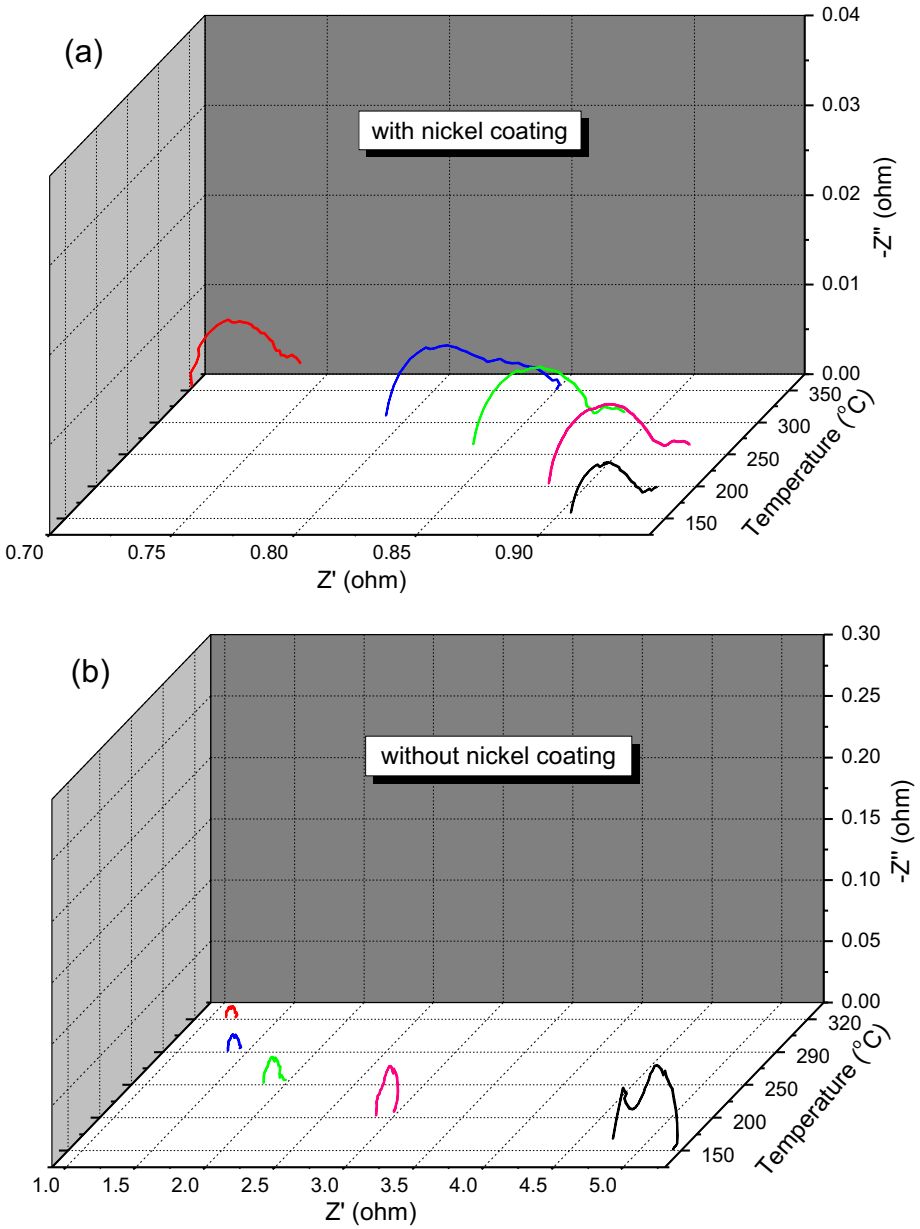

Fig. 12. Impedance spectra of Na/β″-alumina/Na with and without the nickel coating at different temperatures during the cooling process.

and better polarization performance at both high and low current densities. Besides, the potential values of the cell with coating at a given current are smaller than the uncoated one, indicating that the interior resistance of the cell decreases with the nickel coating on account of the improved wettability of the β″-alumina for sodium. The resistance of the cell without coating is not increasing any longer mainly due to the pristine β″-alumina readily wetted by sodium after 6 h polarization, which is consistent with the results reported by Armstrong et al. [28]. In order to investigate the stability of the nickel coating during the cycling, the impedance responses for the Na/β″-alumina/Na cells with and without the nickel coating after polarization are measured as the temperature decreases (Figs. 11 and 12). From the fitting impedance values in Table 1, the interfacial resistances of the two cells are similar at 350 °C caused by the similar wetting behavior, which supports the results of the polarization section. However, as seen in Fig. 12, the interfacial resistances of the cell with coating at lower temperatures are much smaller than those of the cell without coating. For instance, the R_{ct} of the cell with coating is 0.01 Ω compared with 0.095 Ω without coating at 200 °C. It can be proposed that the stable nickel coating after cycling retains favorable wetting behavior at lower temperatures. Our work indicates that the nickel NNC directly coated on the surface of the β″-alumina electrolyte may present a potential solution for the polarization problems at the sodium/β″-alumina interface in Na-beta batteries.

4. Conclusion

In this paper, nickel nanowire network coatings were designed and successfully coated on the surface of the β″-alumina electrolyte through a low-cost and soft-template method. The morphology of the prepared nickel NNCs can be controlled simply by varying the use-level of PMMA. This synthesis method is thought to be extended to any compact substrate with arbitrary shape that is stable under medium temperature. The nickel coating greatly improves the wettability of the β″-alumina ceramic surface for sodium, and has low sheet resistance of ca. 1 Ω sq^{-1}. Moreover, the results of Na/β″-alumina/Na cells at 350 °C reveal that the polarization behavior of the cell is significantly alleviated by the addition of the nickel NNC coating. We anticipate that nickel nanowire network coatings directly coated on the surface of the β″-alumina electrolyte may present a potential solution for the polarization problems at the sodium/β″-alumina interface in Na-beta batteries.

Acknowledgments

The authors appreciate the financial support from the National Natural Science Foundation of China (No. 50730001), the Science and Technology Commission of Shanghai Municipality (No. 08DZ2210900), and Chinese Science and Technology Ministry (No. 2007 CB 209700).

References

[1] C. Liu, F. Li, L.-P. Ma, H.-M. Cheng, Adv. Mater. 22 (2010) E28–E62.
[2] X. Lu, G. Xia, J.P. Lemmon, Z. Yang, J. Power Sources 195 (2010) 2431–2442.
[3] Z. Wen, Y. Hu, X. Wu, J. Han, Z. Gu, Adv. Funct. Mater. 23 (2012) 1005–1018.
[4] J.L. Sudworth, J. Power Sources 100 (2001) 149–163.
[5] J.L. Sudworth, A.R. Tilley, The Sodium Sulphur Battery, Chapman & Hall, London, 1985.
[6] A.C. Buechele, L.C. De Jonghe, Am. Ceram. Soc. Bull. 58 (1979) 861.
[7] A. Imai, M. Harata, Jpn. J. Appl. Phys. 11 (1972) 180–185.
[8] I. Yasui, R.H. Doremus, J. Electrochem. Soc. 125 (1978) 1007–1010.
[9] C.C. Addison, E. Iberson, J. Chem. Soc. (1965) 1437.
[10] R. Knoedler, W. Baukal, W.H. Kuhn, J. Electrochem. Soc. 124 (1977) 236–237.
[11] M.L. Wright, UK Patent Application, 1981, 2067005.
[12] G. Kumar, K.N. Prabhu, Adv. Colloid Interface Sci. 133 (2007) 61–89.
[13] C.A. Leon, R.A.L. Drew, Composites Part A 33 (2002) 1429–1432.
[14] D. Reed, G. Coffey, E. Mast, N. Canfield, J. Mansurov, X. Lu, V. Sprenkle, J. Power Sources 227 (2013) 94100.
[15] Y. Hu, Z. Wen, X. Wu, J. Jun, J. Power Sources 219 (2012) 1–8.
[16] A.R. Madaria, A. Kumar, C.W. Zhou, Nanotechnology 22 (2011) 245201.
[17] L.B. Hu, H.S. Kim, J.Y. Lee, P. Peumans, Y. Cui, ACS Nano 4 (2010) 2955–2963.
[18] X.B. Cao, Y. Xie, L.Y. Li, Adv. Mater. 15 (2003) 1914–1918.
[19] D.H. Wang, H.P. Jakobson, R. Kou, J. Tang, R.Z. Fineman, D.H. Yu, Y.F. Lu, Chem. Mater. 18 (2006) 4231–4237.
[20] D. Walsh, L. Arcelli, T. Ikoma, J. Tanaka, S. Mann, Nat. Mater. 2 (2003) 386–390.
[21] Z. Wen, Z. Gu, X. Xu, J. Cao, F. Zhang, Z. Lin, J. Power Sources 184 (2008) 641–645.
[22] A.T. Rodriguez, X. Li, W.A. Steen, H. Fan, Adv. Funct. Mater. 17 (2007) 2710–2716.
[23] S. Ramesh, G.P. Ang, Ionics 16 (2010) 465–473.
[24] A. Balamurugan, S. Kannan, V. Selvaraj, S. Rajeswari, Trends Biomater. Artif. Organs 18 (2004) 041–045.
[25] M.S. Khan, R.A. Qazi, M.S. Wahid, Afr. J. Pure Appl. Chem. 2 (2008) 041–045.
[26] M.C. Costache, D.Y. Wang, M.J. Heidecker, E. Manias, C.A. Wilkie, Polym. Adv. Technol. 17 (2006) 272–280.
[27] L. Viswanathan, A.V. Virkar, J. Mater. Sci. 17 (1982) 753–759.
[28] R.D. Armstrong, T. Dickinson, J. Turner, Electroanal. Chem. Interfacial Electrochem. 44 (1973) 157–167.